Evaluating spatial dependency of the spectral efficiency in trans-palpebral illumination for widefield fundus photography

Mojtaba Rahimi,[1] **Alfa Rossi,**[1] **Taeyoon Son,**[1] **Devrim Toslak,**[2] **David Le,**[1] **Mansour Abtahi,**[1] **Michael J. Heiferman,**[3] **R. V. Paul Chan,**[3] **and Xincheng Yao**[1,3,*]

[1]*Department of Biomedical Engineering, University of Illinois at Chicago, Chicago, IL 60607, USA*
[2]*Department of Ophthalmology, Antalya Training and Research Hospital, Antalya, Turkey*
[3]*Department of Ophthalmology and Visual Sciences, University of Illinois at Chicago, Chicago, IL 60612, USA*
[*]*xcy@uic.edu*

Abstract: Multi-spectral widefield fundus photography is valuable for the clinical diagnosis and management of ocular conditions that may impact both central and peripheral regions of the retina and choroid. Trans-palpebral illumination has been demonstrated as an alternative to transpupillary illumination for widefield fundus photography without requiring pupil dilation. However, spectral efficiency can be complicated due to the spatial variance of the light property through the palpebra and sclera. This study aims to investigate the effect of light delivery location on spectral efficiency in trans-palpebral illumination. Four narrow-band light sources, covering both visible and near infrared (NIR) wavelengths, were used to evaluate spatial dependency of spectral illumination efficiency. Comparative analysis indicated a significant dependence of visible light efficiency on spatial location, while NIR light efficiency is only slightly affected by the illumination location. This study confirmed the pars plana as the optimal location for delivering visible light to achieve color imaging of the retina. Conversely, spatial location is not critical for NIR light imaging of the choroid.

1. Introduction

Fundus photography is important for the clinical evaluation of ocular pathologies. Despite the availability of advanced imaging modalities such as optical coherence tomography (OCT) and fluorescein angiography (FA), fundus photography remains widely used due to its ease of use, noninvasiveness, and cost-effectiveness [1,2]. Widefield fundus photography is particularly valuable in diagnosing and managing retinal diseases affecting both the central and peripheral regions, such as diabetic retinopathy and peripheral retinal degenerations which may pose a risk of retinal detachment, a severe condition that can lead to blindness [3,4]. Achieving a wide field of view (FOV) is challenging in conventional fundus cameras due to the limit of conventional transpupillary illumination [5]. According to the Gullstrand Principle, separating the illumination and imaging paths for fundus imaging is crucial to avoid severe reflection artifacts at the cornea and crystalline lens, which can significantly degrade fundus image quality [6,7]. Since the available pupil should be carefully shared for illuminating and imaging the same fundus region, traditional fundus photography is limited to a FOV of 30° - 45° visual-angle (45° - 68° eye-angle) [8]. Pupillary dilation and capturing multiple fields of images are necessary to expand the effective FOV to examine the periphery in traditional fundus photography. Miniaturized indirect ophthalmoscopy has been studied to expand the FOV, resulting in a nonmydriatic fundus imaging system capable of achieving a 67° visual-angle (101° eye-angle) FOV [9–12]. Scanning laser ophthalmoscopy (SLO) based imaging systems such as Optomap (Optos, Marlborough, MA,

USA) and Eidon (Icare USA Inc., Raleigh, NC, USA) have been developed to provide widefield fundus photography [2,13]. However, the use of multiple laser sources and scanning systems increases system complexity and device cost.

Trans-pars-planar illumination, as an alternative to transpupillary illumination, has been investigated to expand the FOV in fundus photography without the need for pharmacological pupillary dilation [14–16]. The pars plana, located in the posterior part of the ciliary body, is characterized by a flat structure with comparatively low density of muscle, blood vessels and pigmentation, making it an ideal area for illumination of the fundus. Due to its unique anatomical structure and location, it has been also utilized for various ophthalmic procedures such as drug delivery, vitreoretinal surgery, and diagnostic sample acquisition [17,18].

The utilization of trans-pars-planar illumination for fundus photography relies on the transmission efficiency of light through the sclera and pars plana. The optical properties of the human sclera have been extensively investigated, revealing distinctive wavelength-dependent transmission characteristics [19,20]. In the visible spectrum, the sclera exhibits limited transmission, with higher attenuation towards shorter wavelengths. This behavior is attributed to the absorption by endogenous chromophores, such as melanin and hemoglobin, as well as the scattering effects caused by the scleral microstructure. However, in the near infrared (NIR) range, the sclera demonstrates enhanced transmission, with lower attenuation compared to visible wavelengths. This behavior can be attributed to reduced scattering and lower absorption by scleral tissue in the long wavelength region. Zadorozhnyy et al. [21] proposed visualization of the ciliary body using NIR illumination for transscleral laser cyclodestruction. They showed that the pars plana of the ciliary body can be visualized as a light-wide area between the shadow of the pars plicata and ora serrata. Furthermore, in an ultrasound biomicroscopy image, the pars plana appears slightly brighter than the adjacent sclera [22]. Although there is currently a lack of research specifically focusing on the optical properties of the pars plana, its thin, hypopigmented, and relatively low vascular property suggests that it might exhibit higher light transmission characteristics compared to other areas of the sclera.

Wang et al. [15] and Toslak et al. [23] have reported that the efficiency of trans-pars-planar illumination is location dependent. They have demonstrated that the region outside of the pars plana area experiences a notable decrease in illumination efficiency for visible wavelengths. In contrast, Stepanov et al. [24] have reported no significant variation in illumination efficiency for different locations in transscleral illumination. These discrepancies can be attributed to variations in experimental parameters, such as light wavelengths and illumination spot size, employed across different studies.

Trans-palpebral illumination has also been demonstrated for fundus photography, delivering light through the palpebra and pars plana to eliminate the need for direct contact to the sclera [23,25]. Multispectral imaging (MSI) of the retina and choroid was implemented using narrow-band light emitting diodes (LEDs) [14]. Visible light, especially green light, predominantly uncovers retinal blood vessels, while NIR light illumination reveals the vasculature of the choroid [26,27]. Son et al. [28] demonstrated that the efficiency of light transmission in trans-palpebral illumination significantly depends on wavelength. However, previous studies have not examined the impact of illumination location on trans-palpebral illumination, despite the use of the pars plana as the designated illumination window. The successful implementation of trans-palpebral illumination for widefield fundus photography depends on the effectiveness of the transmitted light. Consequently, there is a knowledge gap regarding the precise understanding of the spectral and spatial properties of trans-palpebral illumination. To address this issue, this study aims to investigate spatial dependency of spectral efficiency in trans-palpebral illumination for widefield fundus photography.

The visual angle has been the FOV unit of traditional fundus cameras. Recently, widefield fundus imagers, such as Optomap (Optos Inc., Marlborough, MA, USA), ICON (Neolight,

Pleasanton, CA, USA), and RetCam (Natus Medical Systems, Pleasanton, CA, USA) use eye angle as the unit of FOV. To avoid unnecessary confusion, both visual angle and eye angle are presented in this article [29].

2. Materials and methods

2.1. Experimental setup

Figure 1 (A) illustrates the optical layout of fundus photography with trans-palpebral illumination. The 22D ophthalmic lens (L_1) (OI-22 M, Ocular Instruments, Inc. Bellevue, WA) creates an aerial image of the retina at the retina conjugate plane, which is relayed to the camera sensor by the camera lens (L_2) (33-303, Edmund Optics Inc., Barrington, NJ). The cross-sectional arrangement of optical fibers in the trans-palpebral illuminator is represented in Fig. 1(B). Five optical fibers with a diameter of 1 mm and a numerical aperture of 0.51 (02–534, Edmund Optics Inc., Barrington, NJ) were utilized. The fibers were positioned with a 0.5 mm interval to deliver light through various palpebral locations. The selected diameter of the fibers ensures an adequate power level, particularly for visible wavelengths. Given that the average size of the pars plana in adults is approximately 4 mm [18], the dimensions of the illuminator were meticulously planned to accommodate this anatomical character. By placing the center channel of the illuminator at the center of the pars plana, two adjacent channels are strategically positioned at the border of the pars plana, while another two edge channels are located outside the pars plana region. This design enables precise investigation of the illuminator location and minimizes the potential impact of inaccuracies caused by displacement and eye movement. Visible and NIR LEDs with center wavelengths of 530 nm (M530L4, Thorlabs Inc, Newton, NJ), 625 nm (M625L4, Thorlabs Inc, Newton, NJ), 780 nm (M780L3, Thorlabs Inc, Newton, NJ), and 970 nm (M970L4, Thorlabs Inc, Newton, NJ) were selected to image the retina and choroid, respectively. A color CMOS camera (DFK 37BUX250, The Imaging Source Europe GmbH, Bremen, Germany) and a monochrome CCD camera (CM3-U3-28S4M-CS, FLIR systems Inc, Wilsonville, OR) were used for fundus photography and pars plana monitoring, respectively. The infrared filter of the color camera was removed to allow NIR light detection. The exposure time for fundus imaging during the study protocol was set to 500 ms and 100 ms for the 530 nm LED and the remaining LEDs, respectively.

2.2. Human subjects and imaging procedures

The Institutional Review Board of the University of Illinois at Chicago approved this study, and it adhered to the ethical guidelines outlined in the Declaration of Helsinki. Three human subjects who were in good health and had no previous eye disease history were recruited for this study. Informed consent was taken from each subject before the experiment.

The images of the fundus were captured in a dark room. To ensure imaging stability, the subject's head was positioned with the forehead and chin placed on support rests (Fig. 1(C)). The trans-palpebral illuminator was placed on the eyelid and a center channel was aligned approximately 4 mm away from the limbus, to be positioned at the pars plana. The location of the trans-palpebral illuminator is monitored using the pars plana camera. The illuminator was fine-tuned for each subject, based on the brightness of a live preview image for optimal position. A custom LabVIEW interface was developed to facilitate real-time viewing to align the fundus camera and trans-palpebral illuminator and capture the fundus images in sequence. To facilitate fixation of the subjects' eyes, a dimly lit LED was used as a visual target during the imaging procedure.

2.3. Light safety

The light safety was assessed for both photochemical and thermal hazards of the retina using the ISO standard "Ophthalmic Instruments- Fundus Cameras" [30]. According to the ISO
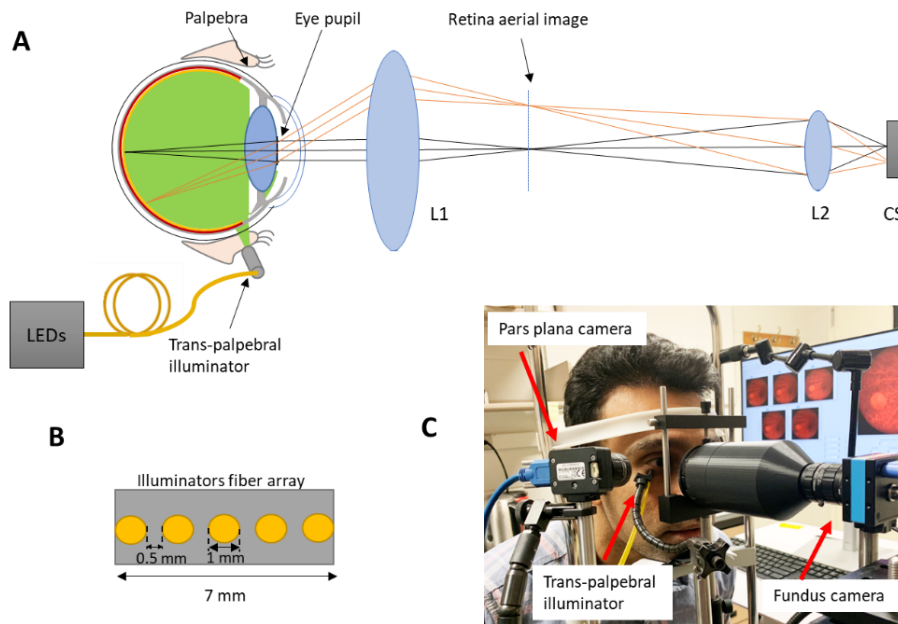
Fig. 1. (A) Schematic diagram of the trans-palpebral illumination-based fundus camera. (B) Schematic diagram of trans-palpebral illuminator with five optical fibers. (C) Photographic illustration of the fundus imaging system. The pars plana camera is utilized to monitor the illumination location.

standard, a radiant exposure of 10 J/cm^2 is allowed on the retina, which is 10 times lower than the threshold for photochemical damage. The ISO standard's photochemical hazard weighting function was utilized to compute the weighted irradiance and maximum permissible exposure time. The illumination power at the fiber output was set as 25 mW, 12 mW, 7 mW, and 4 mW for 530 nm, 625 nm, 780 nm, and 970 nm, respectively. The normalized emission spectrum of the employed LEDs is shown in Fig. 2 (A). In the case of 625 nm and NIR sources, the aphakic photochemical hazard weighing function is less than 0.007, indicating that the photochemical hazard is neglectable. For the 530 nm, the aphakic photochemical hazard weighting function is 0.025 leads to 0.625 mW weighted power [30]. The light emitted from the fiber traverses through the palpebra and sclera to reach the retina. The sclera, located near the corneoscleral limbus, has a thickness of approximately 0.5 mm [31], while the palpebral thickness is about 1.0 mm [32]. With reference to the schematic depicted in Fig. 2 (B) and neglecting the effects of refraction between the surfaces, light scattering and diffusion in the palpebra and sclera, the output light exhibits a divergence angle (θ) of 30.7° for the mostly conservative estimation of light safety. As a result, the illuminated area on the retina is estimated to be about 6 mm^2 and the maximum permissible exposure time is about 5.3 hours. To avoid thermal hazards, the highest weighted power intensity allowed is 700 mW/cm^2 [30]. Based on thermal hazard estimation, the equivalent powers for 530 nm, 625 nm, 780 nm, and 970 nm light sources are 5.6 mW/cm^2, 0.5 mW/cm^2, 5.1 mW/cm^2, and 2.9 mW/cm^2, respectively. The determined weighted power intensity for all wavelengths was found to be below the maximum limit, indicating that there were no thermal hazard concerns for any of the wavelengths considered. The details about the computation of ocular light safety has been explained in previous publication [14].
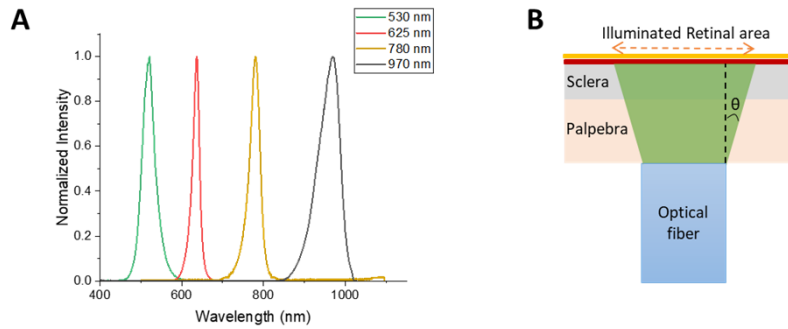
Fig. 2. (A) Visible and NIR LED spectra. (B) Schematic illustration of illuminated retinal area considered for light safety calculation.

3. Results

The anatomical structure and location of the pars plana is shown in Fig. 3 (A). In Fig. 3 (B and C), the pars plana is imaged using visible (625 nm) and NIR (780 nm) wavelength light. The fiber contacts the eyelid on the opposite side, resulting in the transillumination of the eyeball. Both images demonstrate that the brightness of the sclera overlying the pars plana is noticeably greater than other regions of the sclera due to its high transmission property. Furthermore, in the visible image, the boundaries between the pars plana and other scleral regions appear sharper than NIR image due to a greater attenuation of short wavelengths in areas outside of the pars plana. The normalized intensity profiles of the dashed lines are depicted in Fig. 3 (B and C) for quantitative comparison (Fig. 3 (D)). The full width at half maximum (FWHM) of the normalized intensity profile in the visible image is about 3.7 mm which can be considered as the pars plana region and is consistent with the literature [18]. In contrast, the FWHM of NIR image represents ~ 7 mm.
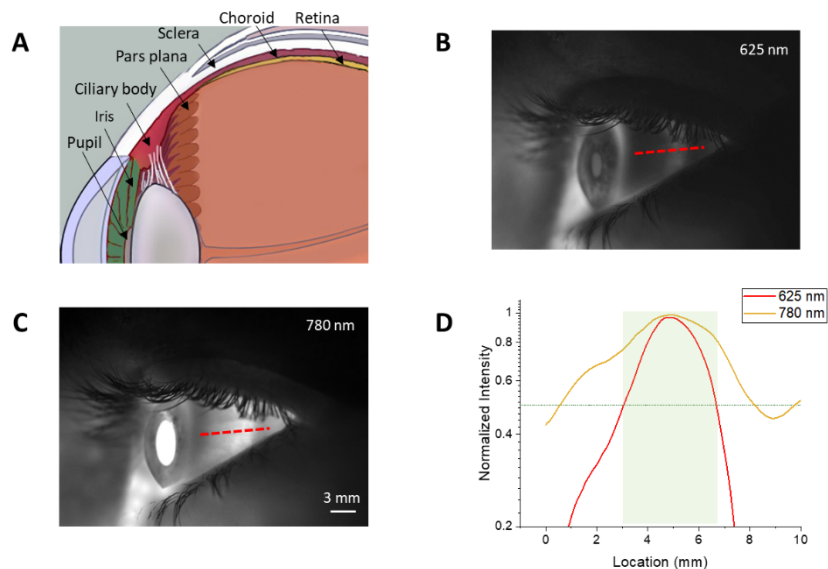

Fig. 3. (A) Schematic drawing of anatomic structure of the human eye [33]. Pars plana images from visible (B) and NIR (C) light. (D) Normalized intensity profile of the red dashed lines shown in (B) and (C).

Figure 4 shows fundus images captured sequentially from the different channel illumination locations with the 625 nm LED. The major retinal features such as optic nerve head, macula and vasculature are observed particularly well when the illuminator is positioned at the pars plana location while the features are ambiguous, and the image brightness gradually decreases when the illuminator is further from the pars plana (Fig. 4 (A)). Similarly, the optimum fundus image is observed when the illuminator is positioned at the pars plana, regardless of the anterior or posterior shift of illuminator (Fig. 4 (B) and (C)). The pars plana location is identified from NIR photograph of the eye and illuminator is shifted 0.5 mm away in each anterior and posterior direction with respect to the pars plana (Fig. 4 (D)).
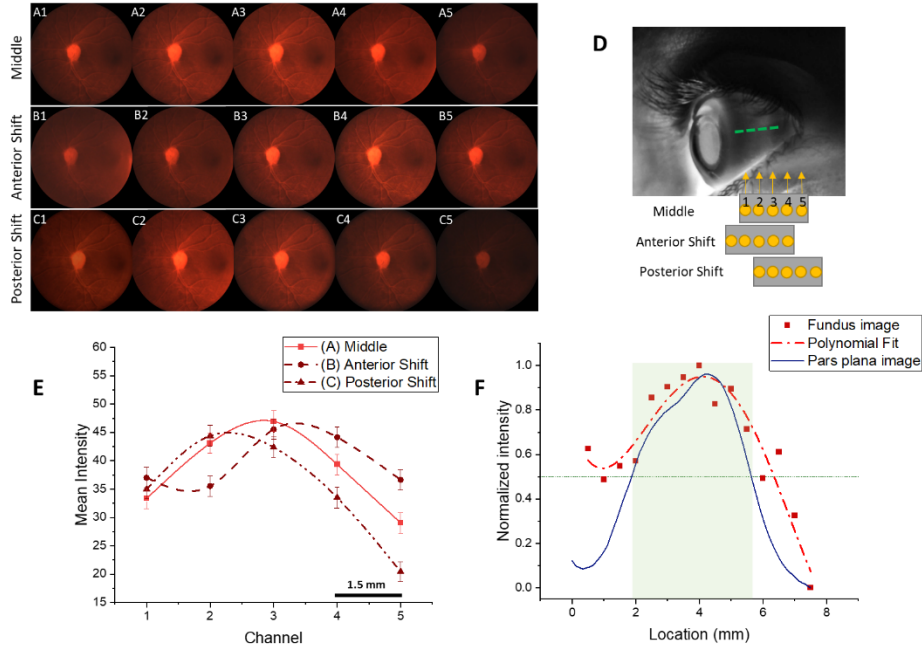

Fig. 4. Representative fundus images from each channel with trans-palpebral illuminator positioned at middle (A), anterior shift (B), and posterior shift (C), respectively. (D) Pars plana image with various illuminator locations. (E) The mean intensity of each fundus images represented in panel (A) through (C). (F) Normalized fundus image intensity and pars plana image intensity of the green dashed line shown in (D).

The brightness of the fundus image is considered as a parameter for the quantitative assessment of spatial location dependence of trans-palpebral illumination efficiency. The brightness of an image (I) is determined by the illumination efficiency (η), illumination power (P), exposure time (t), gain (g), and quantum efficacy (q) of the camera. The relationship can be expressed as [28]:

$$I \propto \eta P t g q \qquad (1)$$

indicating that changes in any of these variables will result in a corresponding change in image brightness. As long as the light source power and camera settings are constant, the image brightness is directly proportional to the illumination efficiency. To evaluate changes in image brightness based on the illumination location, average pixel intensities of each image corresponding to five channels are calculated and illustrated in Fig. 4 (E). The result demonstrates that the overall brightness of the fundus image is significantly higher with pars plana illumination, whereas brightness is gradually degraded in areas outside the pars plana. This confirms that the efficiency of trans-palpebral illumination is dependent on spatial location of the illuminator. By

comparing the variations in brightness of fundus images and the intensity profile of the pars plana across different locations along the sclera (Fig. 4 (F)), it further verifies the superior transparency of the pars plana region compared to other area of the sclera.

The fundus images from multiple visible and NIR wavelengths are presented in Fig. 5 (A-D). For acquiring images in Fig. 5, the channel 3 illumination was adjusted to the center of the para plana, with channel 1 at the anterior side to the limbus as shown in Fig. 4(D). Therefore, relative distances (RDs) of these five illumination channels were estimated at –3.0 mm (channel 1), -1.5 mm (channel 2), 0 mm (channel 3), 1.5 mm (channel 4) and 3.0 mm (channel 5), respectively, from the center of the pars plana. The retinal structures, optics disc, macular, and retinal vessels, are clearly identified in the fundus with the 530 nm green light illumination. (Figure 5 (A)) while the choroidal vessels are revealed using 625 nm and 780 nm (Fig. 5 (B) and (C)). Furthermore, 970 nm illumination visualized choroidal venous structures (Fig. 5 (D)). Notably, a significant difference in image brightness was observed in visible fundus depending on the illumination location whereas NIR fundus shows relatively flat brightness over all illumination locations. The quantitative evaluation of the location sensitivity of trans-palpebral illumination depending on the wavelength was illustrated in Fig. 6. The overall mean intensity is high at longer wavelengths and vice versa which indicates NIR illumination has better illumination efficiency than visible illumination. For visible wavelengths, the image brightness is high with pars plana illumination and considerably decreases at the areas outside of the pars plana. However, the image brightness for NIR illumination shows no significant change regardless of the illumination location. The sharpness of the captured images was quantitatively evaluated using the gradient method, which serves as a no-reference image quality assessment technique [34]. The results, presented in Table 1, demonstrate the extent of image sharpness variation across different channels at visible wavelengths. Remarkably, the analysis reveals an approximately 40% variation in image sharpness for visible wavelengths. In contrast, the variation in image sharpness for NIR wavelengths is found to be less than 10%. These findings show a decrease in image quality for the channels located outside of the pars plana region when using visible wavelengths. It is important to note that enhancing the brightness of channels located outside of the pars plana region using digital image brightness adjustment introduces an unavoidable increase in the image's noise level. To quantify this effect, all images were subjected to histogram matching for brightness alignment, using the channel 3 image as the reference. Subsequently, the noise level for each channel was calculated using the fast noise variance estimation method [35,36], and the results are presented in Table 2. This analysis reveals a substantial increase in the noise level of images located outside the pars plana region when visible wavelengths are utilized. A comparison of images in channel 1 and 5 with the channel 3 image illustrates a 100% increase in noise for the 530 nm wavelength and a 70% increase in noise for the 625 nm wavelength, respectively. In contrast, the variation in noise levels among different channels for NIR images remains below 10%. These findings underscore the degradation in image quality observed for channels located outside the pars plana region when visible wavelengths are employed.

Table 1. Image sharpness measurement[a]

wavelength \ RD[a]	Channel 1 RD = -3.0 mm	Channel 2 RD = -1.5 mm	Channel 3 RD = 0.0 mm	Channel 4 RD = 1.5 mm	Channel 5 RD = 3.0 mm
530 nm	0.679	0. 762	0.955	0.689	0.559
625 nm	0.600	0.668	1.025	0.780	0.586
780 nm	0.735	0.809	0.795	0.791	0.751
970 nm	0.782	0.791	0.814	0.793	0.777

[aa] RD represents relative distance of the illumination location from the center of the pars plana
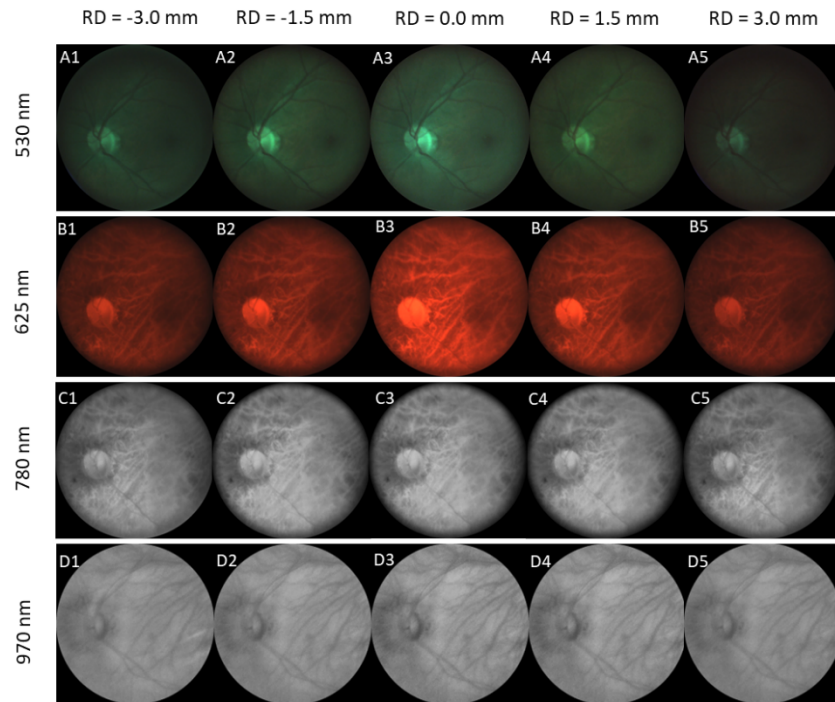
Fig. 5. Representative fundus images from different channel illumination with 530 nm (A), 625 nm (B), 780 nm (C), and 970 nm (D) wavelength. RD represents relative distance of the illumination location from the center of the pars plana.
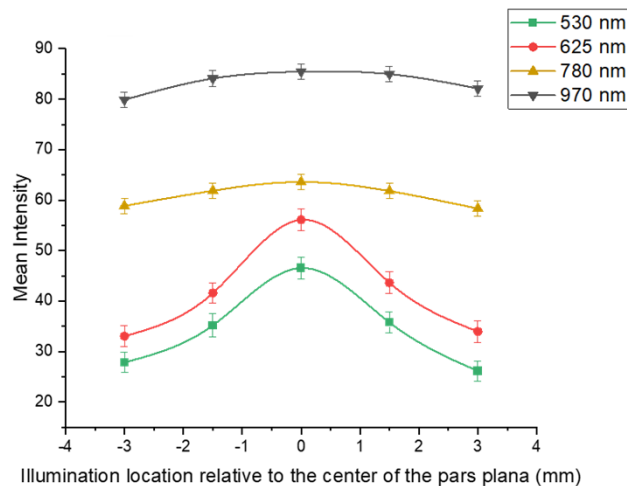

Fig. 6. The mean intensity of fundus images corresponding to panels (A) to (D) in Fig. 5.

In Fig. 7, the mean intensity of fundus images acquired from 530 nm (A), 625 nm (B), 780 nm (C), and 970 nm (D) wavelengths at different channels is presented for comparative evaluation of wavelength dependent location sensitivity of trans-palpebral illumination from three subjects. The variation of mean intensity is observed depending on the subject due to differences in illumination efficiency between individual subjects. However, the overall trend is similar as

Table 2. Image noise measurement after histogram matching

RD wavelength	Channel 1 RD = -3.0 mm	Channel 2 RD = -1.5 mm	Channel 3 RD = 0.0 mm	Channel 4 RD = 1.5 mm	Channel 5 RD = 3.0 mm
530 nm	0.702	0.633	0.330	0.649	0.684
625 nm	0.556	0.555	0.329	0.570	0.566
780 nm	0.215	0.222	0.218	0.219	0.214
970 nm	0.274	0.251	0.249	0.250	0.248

shown in Fig. 6. The consistency of the results across all subjects supports the validity of the study.
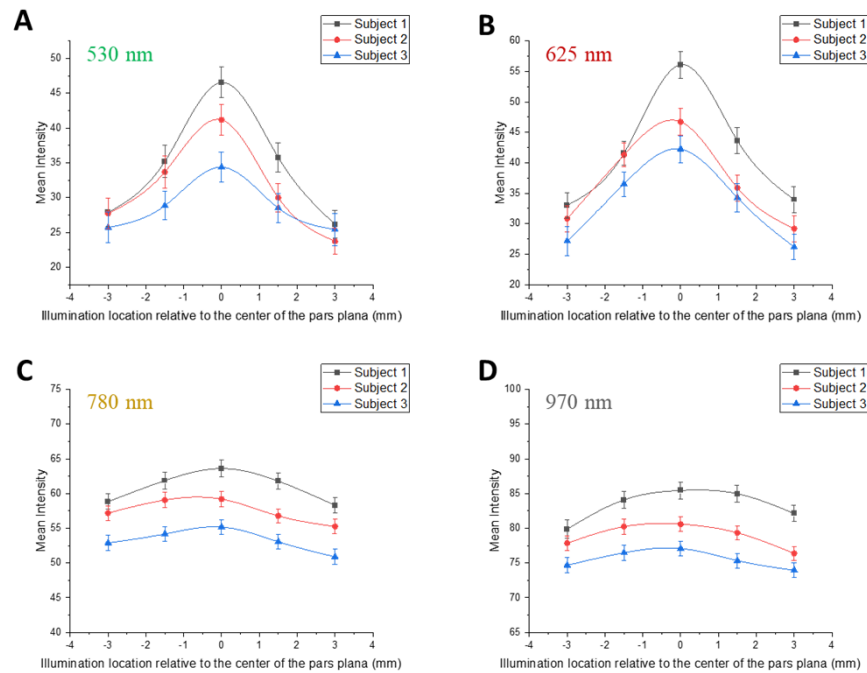

Fig. 7. Comparative evaluation of wavelength dependent location sensitivity of transpalpebral illumination from three subjects. The mean intensity profile of fundus images acquired from 530 nm (A), 625 nm (B), 780 nm (C), and 970 nm (D) wavelength at different channels.

By implementing a carefully controlled balance of 530 nm and 625 nm illuminations, it is possible to generate retinal images that exhibit color representation while also enhancing contrast. The effect of optimal location on the quality of a color-balanced fundus image is demonstrated in Fig. 8. The corresponding fundus images in Fig. 8 (A) are associated with illuminator channels 1, 3, and 5. The overall intensity of channel 3 image is higher compared to the other two channel images corresponding to the illuminator location being outside of the pars plan region. Furthermore, the channel 1 and 5 images manifest a dominance of red tones due to the increased absorption of shorter wavelengths in the area beyond the pars plana. To facilitate a comparison of the visible fundus structures in the color-balanced images, histogram matching is employed, resulting in the images displayed in Fig. 8 (B). Notably, while the channel 3 image, corresponding

to the illuminator situated at the center of the pars plana, vividly reveals both the retinal and choroidal vasculature, a significant portion of the retinal vasculature is obscured in the images linked to illuminators outside of the pars plana region.
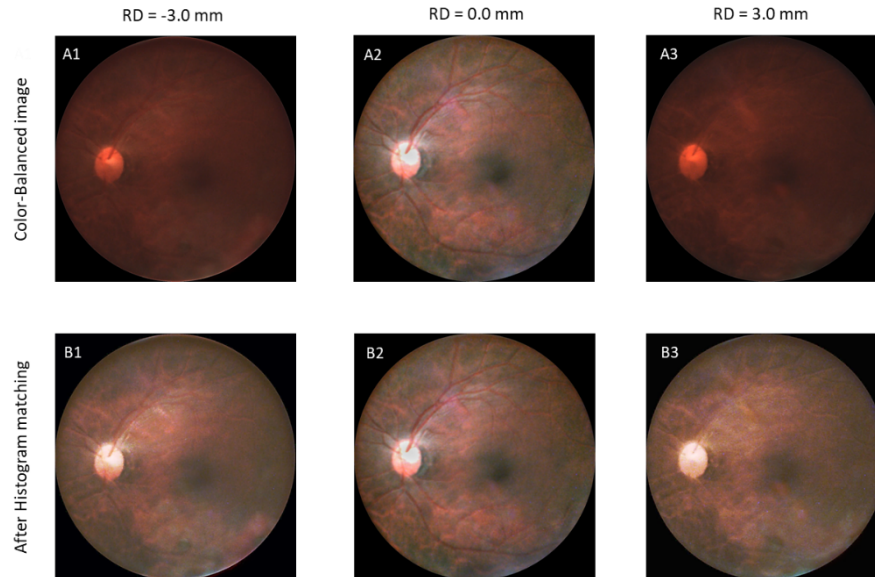

Fig. 8. (A) Color-balanced fundus images from channels 1, 3, and 5 of the trans-palpebral illuminators. (B) Color-balanced fundus images after histogram matching based on the center image.

4.　Discussion

The spatial dependency of spectral efficiency in trans-palpebral illumination for multi-spectral fundus photography was investigated. Illuminating the palpebra with visible and NIR light revealed variations in transparency between the pars plana region and other areas of the sclera. The brightness of the fundus image served as a parameter to quantitatively assess the location dependent efficiency of trans-palpebral illumination for different wavelengths. The results demonstrated a strong spatial dependency when transmitting visible light through the sclera. However, no significant spatial dependency was observed for NIR wavelengths. Image sharpness and image noise level were utilized as no-reference image quality assessment metrics to quantitative evaluate the fundus images quality. The results indicated a decrease in image quality when the illuminator was positioned outside of the pars plana region using visible wavelengths, while there was no noticeable alteration observed for NIR wavelengths.

Multiple studies have reported that the light transmission through the human sclera and eyelid is greater for longer wavelengths, and conversely, lower for shorter wavelengths [37–39]. Furthermore, at visible wavelengths, the transmitted light through the sclera is diffusely scattered, whereas at NIR wavelengths, there is a relatively narrow angular distribution in the forward direction [19]. Consequently, NIR wavelengths exhibit higher transmission through the sclera compared to visible light. This characteristic results in higher illumination efficiency within the NIR range. The pars plana's thin structure and relatively low density of blood vessels contribute to its greater transparency compared to adjacent parts of the sclera. The visualization of the pars plana exhibited greater brightness under both 625 nm and 780 nm wavelengths (Fig. 3 (B) and (C)). However, the boundary of the pars plana appeared more well-defined under visible illumination due to the increased absorption and diffused scattering of shorter wavelengths. Nonetheless, less

absorption and multiple scattering properties associated with NIR wavelengths tend to diminish the sharpness of these borders. When comparing the FWHM of the normalized intensity profile in visible and NIR images (Fig. 3 (D)), it becomes evident that the high transparency region is limited to the pars plana for visible light, while NIR illumination provides relatively high transparency along the entire sclera. This finding highlights the significant impact of location on illumination efficiency when using visible wavelengths.

According to the studies conducted by Wang et al. [15] and Toslak et al. [23], the efficiency of trans-pars-planar illumination is influenced by the location. On the other hand, Stepanov et al. [24] have reported no significant variation in illumination efficiency across different locations of the sclera when employing transscleral illumination. Stepanov et al. [24] utilized a 2.8-mm wide illumination spot on the sclera, with a spacing of 2 to 3 mm between data points. Wang et al. [15] collected images with arc-shaped illumination pattern scanned from the posterior sclera to the limbus at a step interval of ~0.4 mm to show the location dependency for trans-pars-planar illumination. As expected from Fig. 6, increasing the illumination area leads to a decrease in the variation of image brightness. It is worth noting that in both studies, a broadband visible LED (~100 nm bandwidth) was used as the illumination source, which had an impact on the results. In addition, scanning a single illumination across different locations of the sclera might overlook the effect of eye movements during the experiments. To address these issues, narrow spectral band LEDs were utilized in this study to characterize the effect of illumination spectra. Furthermore, an array of illumination points with a fixed distance between them was employed for sequential imaging, which helped to eliminate any inaccuracies caused by eye movements. The results confirmed higher transparency of the pars plana and the significant location dependency of illumination efficiency for visible wavelength.

The utilization of 530 nm illumination primarily visualizes the retinal vasculature, whereas red and NIR illumination unveil the choroidal vasculature. When employing 780 nm light illumination, both arteries and veins in the choroid become visible. However, with 970 nm light illumination, large choroidal veins are revealed (Fig. 5). Son et al. [28] showed that efficiency-balanced visible light illumination is crucial for achieving color retinal imaging via trans-palpebral illumination due to differences in illumination efficiency of different wavelengths. However, when comparing color-balanced images captured with illuminators placed within and outside the pars plana region (Fig. 8), it becomes apparent that illuminators positioned outside of the pars plana region led to the obscuration of the retinal vasculature. This is due to the higher attenuation of shorter wavelengths, which diminishes light necessary to reveal the retinal vasculature in fundus images. Increasing the proportion of green light for illuminators outside the pars plana region poses challenges not only in terms of light safety but also in generating heat on the eyelid, which is uncomfortable for the subject. Therefore, achieving high-quality, color visible fundus images necessitate not only efficiency-balanced illumination but also careful selection of the optimal illumination location.

5.　Conclusion

This study investigated the spatial dependency of spectral efficiency in trans-palpebral illumination for widefield fundus photography. Experimental results indicated that the choice of illumination wavelength and location is critical for capturing high-quality fundus images. Shorter visible light wavelengths improve retinal structure visualization, while longer NIR wavelengths provide clearer choroidal structure visualization. Furthermore, the location of illumination significantly affects the efficiency of visible light, whereas no significant location dependency was observed for NIR light. The pars plana is identified as the optimal location for delivering visible light to the posterior part of the eye. These findings suggest that trans-palpebral illumination can provide an easy and practical illumination approach for choroidal imaging. However, for visible fundus images the optimal location for illumination should be selected to achieve a high-quality fundus

image. This study could pave the way for the development of more practical and efficient widefield fundus imaging systems, enabling the early detection and treatment of ocular pathologies.

Disclosures. No competing interest exists for any author.

Data availability. Data may be obtained from the authors upon reasonable request.

References

1. A. Nagiel, R. A. Lalane, S. R. Sadda, and S. D. Schwartz, "Ultra-widefield fundus imaging: a review of clinical applications and future trends," Retina **36**(4), 660–678 (2016).
2. S. N. Patel, A. Shi, T. D. Wibbelsman, and M. A. Klufas, "Ultra-widefield retinal imaging: an update on recent advances," Therapeutic advances in ophthalmology **12**, 251584141989949 (2020).
3. P. S. Silva, J. D. Cavallerano, N. M. N. Haddad, H. Kwak, K. H. Dyer, A. F. Omar, H. Shikari, L. M. Aiello, J. K. Sun, and L. P. Aiello, "Peripheral lesions identified on ultrawide field imaging predict increased risk of diabetic retinopathy progression over 4 years," Ophthalmology **122**(5), 949–956 (2015).
4. H. Lewis, "Peripheral retinal degenerations and the risk of retinal detachment," Am. J. Ophthalmol. **136**(1), 155–160 (2003).
5. X. Yao, T. Son, and J. Ma, "Developing portable widefield fundus camera for teleophthalmology: Technical challenges and potential solutions," Exp. Biol. Med. **247**(4), 289–299 (2022).
6. A. Gullstrand, "Neue methoden der reflexlosen ophthalmoskopie," Berichte Deutsche Ophthalmologische Gesellschaft **36**, 326 (1910).
7. E. DeHoog and J. Schwiegerling, "Optimal parameters for retinal illumination and imaging in fundus cameras," Appl. Opt. **47**(36), 6769–6777 (2008).
8. N. Panwar, P. Huang, J. Lee, P. A. Keane, T. S. Chuan, A. Richhariya, S. Teoh, T. H. Lim, and R. Agrawal, "Fundus photography in the 21st century—a review of recent technological advances and their implications for worldwide healthcare," Telemedicine and e-Health **22**(3), 198–208 (2016).
9. D. Toslak, C. Liu, M. N. Alam, and X. Yao, "Near-infrared light-guided miniaturized indirect ophthalmoscopy for nonmydriatic wide-field fundus photography," Opt. Lett. **43**(11), 2551 (2018).
10. A. Rossi, M. Rahimi, D. Le, T. Son, M. J. Heiferman, R. V. P. Chan, and X. Yao, "Portable widefield fundus camera with high dynamic range imaging capability," Biomed. Opt. Express **14**(2), 906–917 (2023).
11. A. Rossi, T. Son, M. Rahimi, and X. Yao, "Miniaturized indirect illumination with light polarization and power controls for high dynamic range fundus photography," in *Ophthalmic Technologies XXXIII* (SPIE 2023), pp. 167–172.
12. X. Yao, A. Rossi, T. Son, M. Rahimi, and R. Chan, "Preserving polarization maintaining photons for enhanced contrast imaging of the retina," (2023).
13. Y. Kato, M. Inoue, and A. Hirakata, "Quantitative comparisons of ultra-widefield images of model eye obtained with Optos® 200Tx and Optos® California," BMC Ophthalmol. **19**(1), 115 (2019).
14. D. Toslak, T. Son, M. K. Erol, H. Kim, T.-H. Kim, R. P. Chan, and X. Yao, "Portable ultra-widefield fundus camera for multispectral imaging of the retina and choroid," Biomed. Opt. Express **11**(11), 6281 (2020).
15. B. Wang, D. Toslak, M. N. Alam, R. Chan, and X. Yao, "Contact-free trans-pars-planar illumination enables snapshot fundus camera for nonmydriatic wide field photography," Sci. Rep. **8**(1), 8768 (2018).
16. D. Toslak, F. Chau, M. K. Erol, C. Liu, R. P. Chan, T. Son, and X. Yao, "Trans-pars-planar illumination enables a 200 ultra-wide field pediatric fundus camera for easy examination of the retina," Biomed. Opt. Express **11**(1), 68 (2020).
17. L. Bye, N. Modi, and M. Stanford, "*Basic sciences for ophthalmology*," (OUP Oxford, 2013), p. 51.
18. C. S. Foster and A. T. Vitale, "*Diagnosis & treatment of uveitis*," (JP Medical Ltd, 2013), p. 11.
19. A. Vogel, C. Dlugos, R. Nuffer, and R. Birngruber, "Optical properties of human sclera, and their consequences for transscleral laser applications," Lasers Surg. Med. **11**(4), 331–340 (1991).
20. B. Nemati, H. G. Rylander, and A. J. Welch, "Optical properties of conjunctiva, sclera, and the ciliary body and their consequences for transscleral cyclophotocoagulation," Appl. Opt. **35**(19), 3321–3327 (1996).
21. O. Zadorozhnyy, A. Korol, A. Nevska, T. Kustryn, and N. Pasyechnikova, "Ciliary body imaging with transpalpebral near-infrared transillumination–a pilot study," Klinika Oczna/Acta Ophthalmologica Polonica **118**, 184–186 (2016).
22. Y. Okamoto, F. Okamoto, S. Nakano, and T. Oshika, "Morphometric assessment of normal human ciliary body using ultrasound biomicroscopy," Graefe's Arch. Clin. Exp. Ophthalmol. **255**(12), 2437–2442 (2017).
23. D. Toslak, D. Thapa, Y. Chen, M. K. Erol, R. P. Chan, and X. Yao, "Trans-palpebral illumination: an approach for wide-angle fundus photography without the need for pupil dilation," Opt. Lett. **41**(12), 2688 (2016).
24. A. Stepanov, J. Thorstensen, and J. Tschudi, "Impact of illumination spectrum and eye pigmentation on image quality from a fundus camera using transscleral illumination," J. Biomed. Opt. **26**(07), 076003 (2021).
25. M. Rahimi, A. Rossi, T. Son, and X. Yao, "High dynamic range fundus camera with trans-palpebral illumination," Invest. Ophthalmol. Visual Sci. **64**, 5016 (2023).

26. Z. Huang, Z. Jiang, Y. Hu, D. Zou, Y. Yu, Q. Ren, G. Liu, and Y. Lu, "Retinal choroidal vessel imaging based on multi-wavelength fundus imaging with the guidance of optical coherence tomography," Biomed. Opt. Express **11**(9), 5212 (2020).

27. X. Feng, Y. Yu, D. Zou, Z. Jin, C. Zhou, G. Liu, J. G. Fujimoto, C. Li, Y. Lu, and Q. Ren, "Functional imaging of human retina using integrated multispectral and laser speckle contrast imaging," J. Biophotonics **15**(2), e202100285 (2022).

28. T. Son, J. Ma, D. Toslak, A. Rossi, H. Kim, R. P. Chan, and X. Yao, "Light color efficiency-balanced trans-palpebral illumination for widefield fundus photography of the retina and choroid," Sci. Rep. **12**(1), 13850 (2022).

29. X. Yao, D. Toslak, T. Son, and J. Ma, "Understanding the relationship between visual-angle and eye-angle for reliable determination of the field-of-view in ultra-wide field fundus photography," Biomed. Opt. Express **12**(10), 6651 (2021).

30. I. O. f. Standardization, "Ophthalmic Instruments-Fundus Cameras-International Standard, ISO 10940," (2007).

31. T. W. Olsen, S. Y. Aaberg, D. H. Geroski, and H. F. Edelhauser, "Human sclera: thickness and surface area," Am. J. Ophthalmol. **125**(2), 237–241 (1998).

32. P. B. Labib AM and C. Milroy, "Lower Eyelid Laxity Examination," https://www.ncbi.nlm.nih.gov/books/NBK576403/.

33. Wikipedia, "Human eye," https://en.wikipedia.org/wiki/Human_eye.

34. T. Birdal, "Sharpness Estimation From Image Gradients," MatLab, 2023, https://www.mathworks.com/matlabcentral/fileexchange/32397-sharpness-estimation-from-image-gradients.

35. J. Immerkaer, "Fast noise variance estimation," Computer vision and image understanding **64**(2), 300–302 (1996).

36. T. Birdal, "Fast Noise Estimation in Images," Matlab, 2023, https://www.mathworks.com/matlabcentral/fileexchange/36941-fast-noise-estimation-in-images.

37. H. S. Hwang, Y. Xie, E. Koudouna, K.-S. Na, Y.-S. Yoo, S.-W. Yang, D. J. Brown, and J. V. Jester, "Light transmission/absorption characteristics of the meibomian gland," The ocular surface **16**(4), 448–453 (2018).

38. A. Bierman, M. G. Figueiro, and M. S. Rea, "Measuring and predicting eyelid spectral transmittance," J. Biomed. Opt. **16**(6), 067011 (2011).

39. A. Bashkatov, E. Genina, V. Kochubey, and V. Tuchin, "Optical properties of human sclera in spectral range 370–2500 nm," Opt. Spectrosc. **109**(2), 197–204 (2010).